Microelectronics Reliability 54 (2014) 2754–2759

Contents lists available at ScienceDirect

Microelectronics Reliability

journal homepage: www.elsevier.com/locate/microrel

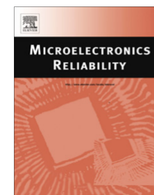

Nanotribological properties of ALD-processed bilayer TiO_2/ZnO films

Wun-Kai Wang [a], Hua-Chiang Wen [b], Chun-Hu Cheng [c], Ching-Hua Hung [a], Wu-Ching Chou [b], Wei-Hung Yau [d,*], Ping-Feng Yang [e], Yi-Shao Lai [e]

[a] Department of Mechanical Engineering, National Chiao Tung University, Hsinchu 300, Taiwan, ROC
[b] Department of Electrophysics, National Chiao Tung University, Hsinchu 300, Taiwan, ROC
[c] Department of Mechantronic Technology, National Normal University, Taipei 106, Taiwan, ROC
[d] Department of Mechanical Engineering, Chin-Yi University of Technology, Taichung 400, Taiwan, ROC
[e] Central Labs, Advanced Semiconductor Engineering, Inc., 26 Chin 3rd Rd., Nantze Export Processing Zone, 811 Nantze, Kaohsiung, Taiwan, ROC

A R T I C L E I N F O

Article history:
Received 27 February 2014
Received in revised form 27 July 2014
Accepted 28 July 2014
Available online 12 September 2014

Keywords:
CVD coatings
Nanotribology
Scratch testing
Sliding friction

A B S T R A C T

TiO_2/ZnO films grown by atomic layer deposition (ALD) demonstrated nanotribological behaviors using scratch testing. TEM profiles obtained an amorphous structure TiO_2 and nanocrystalline structure ZnO, whereas the sample has significant interface between the TiO_2/ZnO films. The experimental results show the relative XRD peak intensities are mainly contributed by a wurtzite oxide ZnO structure and no signal from the amorphous TiO_2.

With respect to tribology, increased friction causes plastic deformation between the TiO_2 and ZnO films, in addition to delamination and particle loosening. The plastic deformation caused by adhesion and/or cohesion failure is reflected in the nanoscratch traces. The pile-up events at a loading penetration of 30 nm were measured at 21.8 μN for RT, 22.4 μN for 300 °C, and 36 μN for 400 °C. In comparison to the other conditions, the TiO_2/ZnO films annealed at 400 °C exhibited higher scratch resistance and friction with large debris, indicating the wear volume is reduced with increased annealing temperature and loading.

© 2014 Elsevier Ltd. All rights reserved.

1. Introduction

Atomic layer deposition (ALD) is regularly selected to produce extremely thin coatings because of its remarkable self-limiting nature and low growth temperature. Many semiconductor materials, such as TiO_2, ZnO, SnO, and Al_2O_3, can be produced by ALD [1–3]. Example materials of TiO_2 and ZnO are based on the following binary CVD reactions and their corresponding reaction enthalpies [4,5]. ZnO is a metal oxide with the property of optical transparency that can be used for applications in optical semiconductor devices or thin-film transistors [6,7]. These material properties have been thoroughly investigated with respect to numerous processing parameters and conditions [8]. Additionally, the selective deposition of TiO_2 by ALD has been reported using polymer masking layers [9,10]. Similarly, the optical properties of these biological replicas have been reported as functions of TiO_2 ALD thickness. [11] Both materials are commonly used because they possess similar band gaps, although the electron mobility of ZnO is higher than that of TiO_2 [12–14].

Novel films have also been studied using ALD for the evaluation of their optical properties. In comparison to single-crystal bulk materials, the deformation properties of thin films processed by ALD are strongly correlated with geometrical dimensions and material defect structures [15]. Thus, the investigation of nanotribological behaviors including the adhesion/cohesion mechanisms of ALD-processed thin films with post-annealing treatments is intriguing. Tribological behaviors are evaluated based on the sliding wear characteristics that are also important for reliability [16–18].

The friction coefficient and volume loss are generally measured from both lubricated and unlubricated conditions at different sliding speeds and distances [19,20]. Related experiments have been conducted using this analytical approach, which exhibits some advantages, such as the free selection of materials, ease in altering the design, and convenient initial facilities [21–23]. Similarly, ALD coating layers can be estimated using the artificial lateral force of scratching to extend the tribological problem for reliability issues. Even now, the research using this approach for the analysis of scratch resistance and adhesion/cohesion failure mechanisms of TiO_2/ZnO films grown by ALD remains far from conclusive.

* Corresponding author. Tel.: +886 423924505; fax: +886 423930681.
E-mail address: ywhung1@gmail.com (W.-H. Yau).

http://dx.doi.org/10.1016/j.microrel.2014.07.148
0026-2714/© 2014 Elsevier Ltd. All rights reserved.

The present paper reports a systematic experimental study on the effect of annealing TiO_2/ZnO films with respect to reliability. Our main goal in this study was to investigate the tribological and microstructural behaviors of the films. The qualities of the resulting films, in terms of the nanoscratch induced deformation, were examined.

2. Experimental details

TiO_2/ZnO films were deposited on Si (1 0 0) substrates using an ALD system operated with the flow-rate interruption method. The wafer was transferred into an ALD reactor in which diethylzinc and water were used as precursors under a processing temperature of 200 °C, and the deposition rate was controlled at 0.2 Å/cycle for ZnO film deposition [6]. The deposition depth ZnO thin film is 30 nm. Subsequently, each ZnO/Si sample was delivered to another chamber for TiO_2 deposition using $TiCl_4$/H_2O precursors with a stable flow rate of 0.7 Å/cycles at 200 °C. Since the ALD-processed films showed only a small thickness variation, the thickness of the stacked film could be easily controlled [24]. After that, a bilayer sample of 10 nm TiO_2 and 30 nm ZnO on a Si substrate was obtained so-called as-deposited condition (RT). Finally, these samples were annealed at temperatures of 300 °C and 400 °C for 1 h in ambient nitrogen with a heating rate of 20 °C/s.

The crystallinity of the TiO_2/ZnO films was analyzed by X-ray diffraction (PANalytical X'Pert Pro (MRD), with Cu Kα (λ = 0.154 nm) radiation for 2θ from 20° to 60° at a scan speed of 2°min^{-1} and a grazing angle of 0.5° under 30 kV and 30 mA. The XRD results were compared to the Joint Committee on the Powder Diffraction Standard Card (JPCDS). A Dimension 3100 scanning probe microscope (SPM, Veeco di-Innova) was utilized with both standard and advanced SPM imaging modes to measure the surface characteristics of the ALD TiO_2/ZnO films. The nanotribological properties of the TiO_2/ZnO films were determined with scanning probe microscopy (SPM, Hysitron Corporation), which was combined with AFM (Digital Instruments Nanoscope III) into a nanoscratch measurement system. The nanoindentation measurements used a diamond Berkovich indenter tip (tip radius ~50 nm), suggesting plastic deformation can be generated at a very small load. Laterally, the probe-sample interaction extends only across the tip atom or the atoms involved in the interaction; additionally, the SPM was operated at a constant scan speed of 2 μm s^{-1}. For the TiO_2/ZnO films, the applied load function was ramped depth mode, and penetrations of 30 nm and 150 nm were examined at room temperature. The maximum load was then maintained while forming 10 μm long scratches. Reliability performance measurements randomly sampled nine positions made on each film. Surface profiles before and after scratching were obtained by scanning the tip at a 0.02-mN normal load (i.e., a load sufficiently small that it produced no measurable displacement). After scratching, the wear tracks were imaged using AFM.

3. Results and discussion

To understand the effect of temperature on the bilayer TiO_2/ZnO films on Si substrates, XRD analysis was used to examine the film phase. The XRD patterns in Fig. 1(a) present crystallization peaks at 2=31.5°, 34° and 36°, which give clear evidence of crystallized ZnO with (1 0 0), (0 0 2), and (1 0 1) crystallographic planes, according to the reference data of JPCDS No. 79-0206 [6]. Fig. 1(b) presents a cross-sectional TEM image of the bilayer TiO_2/ZnO films on Si substrates that have been subjected to RT. A bilayer sample of 10 nm TiO_2 and 30 nm ZnO on a Si substrate was obtained. Fig. 1(c) shows the high resolution TEM profiles obtained an amorphous structure TiO_2 and nanocrystalline structure ZnO, whereas the sample has significant interface between the TiO_2/ZnO films. First, it can be seen the as-deposited TiO_2/ZnO films processed at 200 °C show no TiO_2 peak [25]. To explain the surface morphology of TiO_2/ZnO film before scratching, AFM measurements were carried out, as shown in Fig. 2(a) and (c). It can be seen the surface roughness (R_a) values are 1.8, 1.5 and 1.4 nm for the RT and post-annealed (at 300 and 400 °C) samples, respectively, which exhibit uniform and fine-grained morphology. With increased annealing temperature, the non-stoichiometric surface may create defects or/and nanoparticles [26] as a result of thermally induced crystallization effects

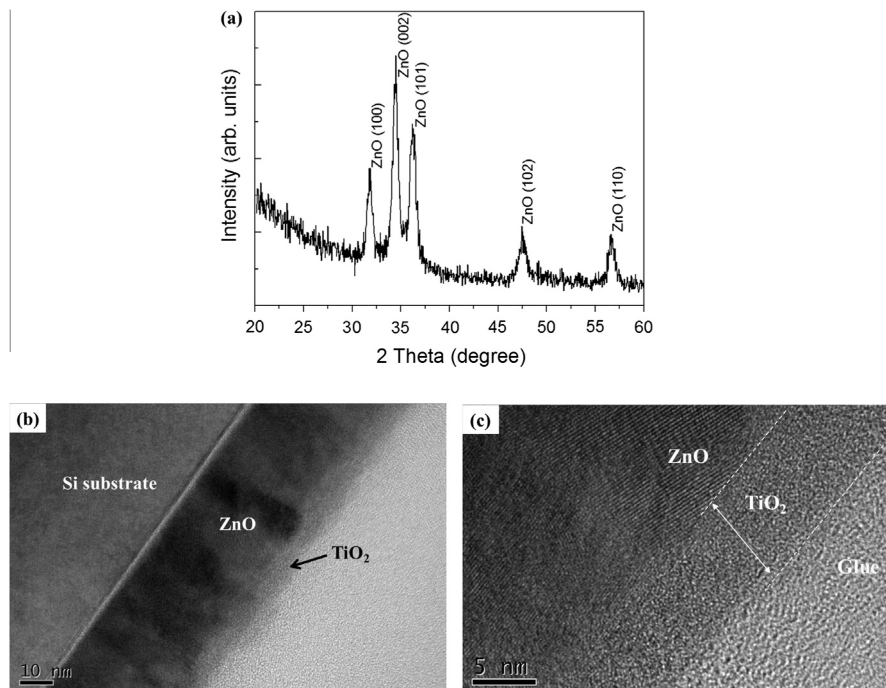

Fig. 1. (a) An XRD pattern of the TiO_2/ZnO films with and without annealing. (b) and (c) TEM profiles obtained a significant interface between of the TiO2/ZnO films.

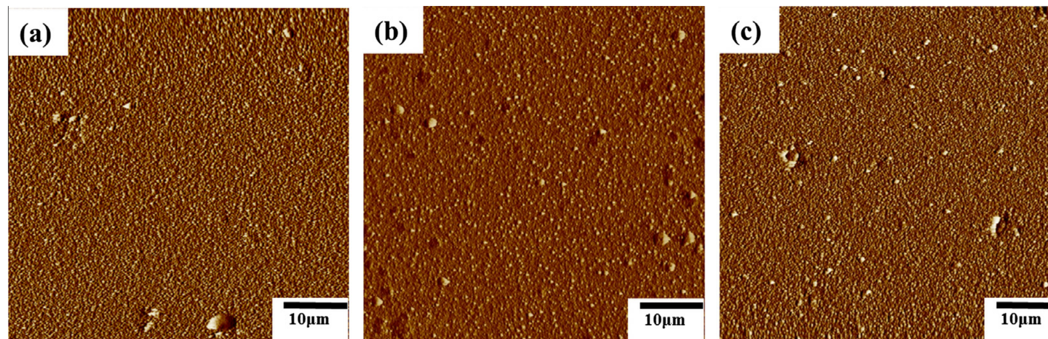

Fig. 2. The surface morphologies of the TiO_2/ZnO films at (a) RT, (b) 300 °C and (c) 400 °C before scratching.

[27]. However, the generation of defect areas should significantly lower the mobility of transport carriers through the bulk [28].

Fig. 3(a) and (b) show typical AFM profiles with varying penetration at 30 nm and 150 nm, respectively. The wear volume increases with time for ALD films fabricated under the RT condition, and it can be observed the total volume was swiped by the indenter, which depended on the projected area of the indenter during application of the scratching test [23,29]. The typical surface morphology with a smooth plane and no fibers is obtained at a ramped loading penetration of 30 nm; additionally, a small amount of debris on the surrounding surface can be observed. Further, the grinding cracks and debris can clearly be found at the last tracking line, which had a penetration of 150 nm. Fig. 3(c) and (d) reveal scratched groove morphologies under a ramped loading test for the sample with a given annealing temperature of 300 °C. However, the use of an appropriate annealing treatment can remove defects, which may have originated from dangling oxide bonds present near the surface or interface, following the ALD process with layer-by-layer deposition. The annealing process also provides enough activation energy for atoms to diffuse into stable atomic sites in the crystal lattice [30]. Thus, the friction surface appears smooth and without debris following the penetration test from 30 to 150 nm. The possible reason for this may be the edge of the friction film becomes tough, improved by the application of an annealing treatment at 300 °C. Fig. 3(e) and (f) reveal scratch groove morphologies in the samples thermally treated at the higher temperature of 400 °C. The smooth tracking line can only be obtained at the light loading penetration of 30 nm; however, a clearly deep track occurred at the penetration of 150 nm, followed by the development of severe debris with particle-gathering morphologies. Thus, we found the occurrence of debris on the edge of the friction film [28,29] depended on the temperature of the annealing treatment. Additionally, it is believed the contact and true volume values increase with the *in-situ* loading force. The related investigations will be discussed in the following content, including a comparison of the data collected for the friction and lateral force curves.

Fig. 4 shows the lateral force as a function of the duration of displacement. It can be observed the applied lateral loading increased with scratching time. In Fig. 4(a), with a loading penetration of 30 nm, the unstable lateral force can be observed with increasing time. However, the samples treated with annealing temperatures of 300 °C and 400 °C exhibit some degree of intermittence under force testing. This appears to be reflected by the fluctuation. The loading condition associated with this event is called the "critical load," and the uncertainty of the displacement profile is called "pile-up" [31,32]. In Fig. 4(b), unusual lateral force behavior can be observed for the sample at the duration of 18–19 s, due to the film pile-up and the measured critical loads of 21.8, 22.4, 36 μN. In comparison to the loading test results for the other conditions, i.e., treatment at RT and 300 °C, the fluctuation is lower. According to the combined plastic deformation of ZnO by intra film shear (slip) of partial dislocations along the ZnO {0002}, basal stacking faults via a dislocation glide process contribute to a lowering of friction and wear [33]. Fig. 5(a) was recorded at a loading penetration of 30 nm; the friction traces can clearly be observed for each sample. The absence of the load and unloading segments of the load–displacement curve suggests ten times pressure-induced was involved by nanoscratch traces (Fig. 6). The parallel measurements to ensure reproducibility can be given by SPM modes to measure the reliability performance of the ALD TiO_2/ZnO films. In addition, the penetration distance can be well controlled to contact the TiO_2 films and not the ZnO films. The plots recorded at the loading conditions of RT, 300 °C, and 400 °C indicate the oscillation trend occurred continuously under the friction force after the setting down step. Consequently, the oscillation trends are similar for each sample, in both the on- and off-load scans at the duration of 19 s. The data recorded at the RT loading condition exhibited more oscillating fluctuations than those recorded at the loading conditions of 300 °C and 400 °C, as can be observed in Fig. 5(b). However, an unusual forcing profile is apparent under RT. Fig. 3 shows an

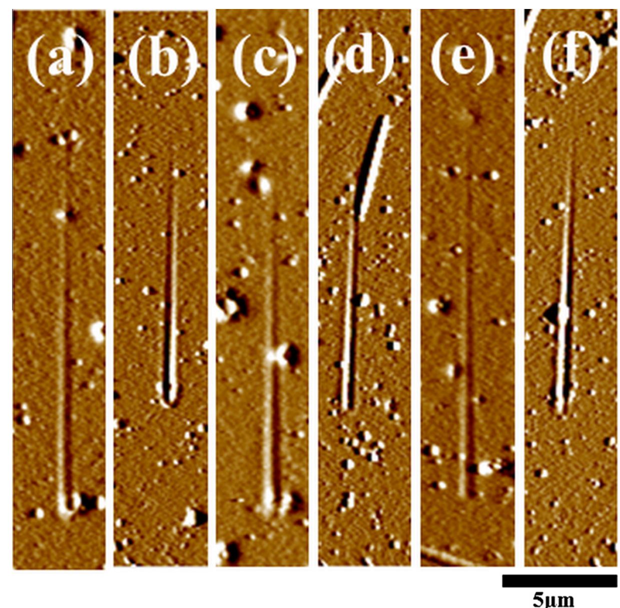

Fig. 3. The surface morphologies of the TiO_2/ZnO films under different annealing conditions after the nanoscratch tests. The RT samples without annealing, subjected to ramped loads of 500–2000 μN, are shown in (a) and (b), The samples treated with the annealing temperature of 300 °C, are shown in (c)-(d), annealing temperature of 400 °C, are shown in (e) and (f), respectively.

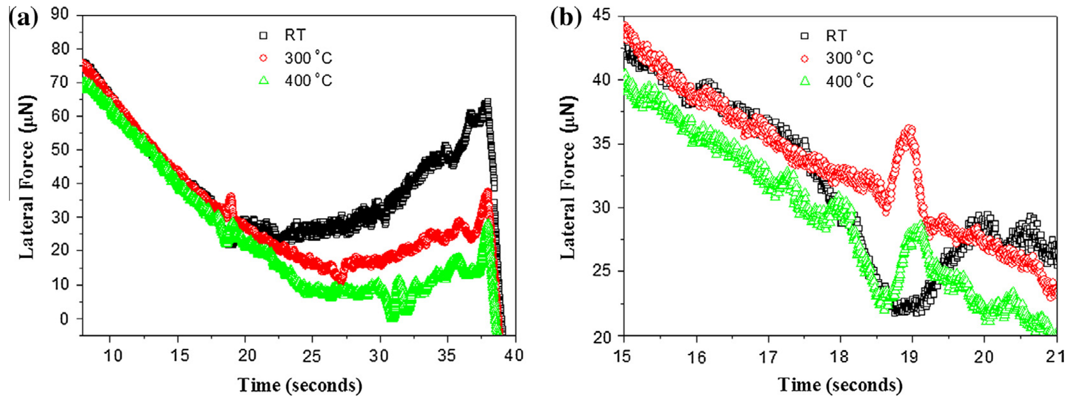

Fig. 4. Three typical profiles of the coefficient of friction (μ) as a function of scratch duration for the TiO_2/ZnO films treated under different annealing conditions of RT, 300, and 400 °C. Ramped loads of (a) 500 μN and (b) zoom for (a).

elastic reaction occurs, caused by elastic deformation between the groove and film after high-temperature annealing. This sample was plowed by indenter tips; this result could be expected because the use of a higher annealing temperature increases film crystallization. Hence, the tip can extend the dislocations in addition to the contact asperities, leading to the occurrence of elastic formation on the TiO_2/ZnO films. It can be seen the lower degrees of adhesion reflect interlinking, and rearrangement tends to result in fluctuations in the values of μ at the ZnO film. Following the uncertainty of the initial μ profile, pile-up occurred in Fig. 5(b), which was recorded at the annealed conditions of 300 °C and 400 °C. The coefficient of friction profiles are generated as a function of the increased loading penetration of 30 nm. The marked oscillations under the friction force and abrupt oscillations can be observed at the conditions of RT in comparison to that of 300 °C and 400 °C. We summarized the ploughed and scratched data under critical loads, as measured from the TiO_2/ZnO films with different penetrations at 150 nm and annealing temperature, presented in Fig. 5(c) for comparison. According to the above experimental results, the annealing temperature affects the nanotribological behaviors, including the plastic deformation between the TiO_2 and ZnO films, delamination and particle loosening. We also confirmed the microstructure of the TiO_2/ZnO films changed as the annealing temperature was increased from 300 °C to 400 °C, causing changes in the composition of the bilayer structure. The failure mechanism during scratching of the TiO_2/ZnO films at the respective critical loads is shown in Fig. 5(c). Note, no critical pile-up occurs at RT or for the annealing conditions of 300 °C and 400 °C.

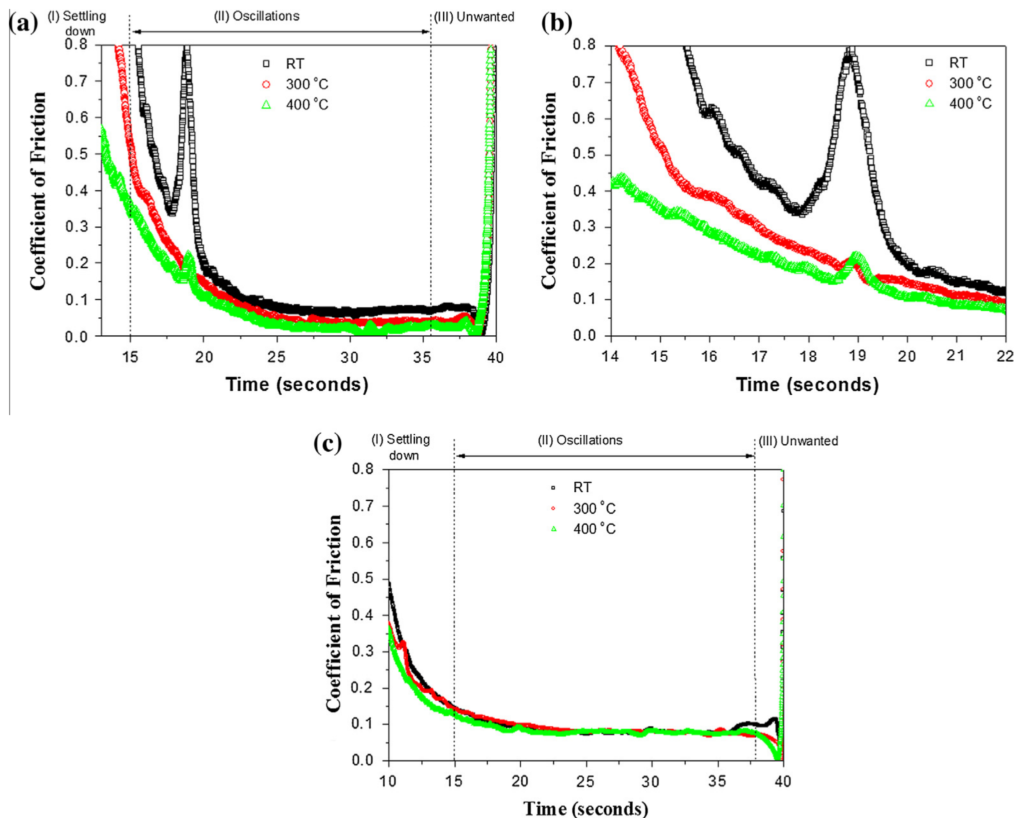

Fig. 5. shows the lateral force as a function of the displacement duration. It can be observed the applied lateral loads increase with testing time for the three samples (RT, 300 °C and 400 °C) with ramped loads of (a and b) 500 and (c) 2000 μN.

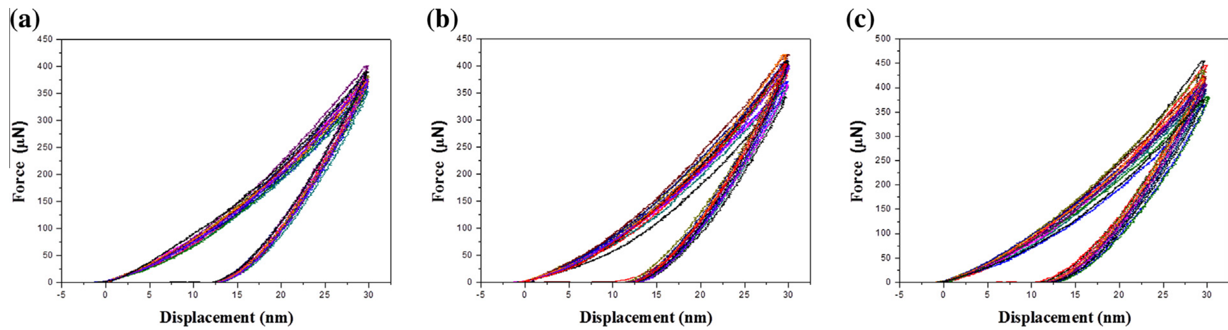

Fig. 6. shows the ten times load and unloading segments of the load–displacement curve by nanoscratch traces.

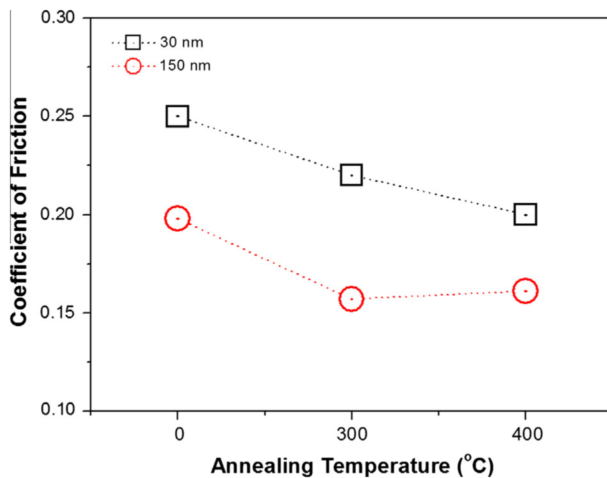

Fig. 7. The distinct critical coefficients of friction as a function of ramped loads of 500 and 2000 μN for TiO_2/ZnO films with processing conditions of RT, 300 °C and 400 °C.

The values of μ were recorded from the TiO_2/ZnO films with respect to the annealing temperature; these values of μ were determined by averaging the values measured at scratch durations ranging from 15 to 36 s (Fig. 7).

The obtained discordant curves and irregularities appeared in the course of plastic deformation as a result of the adhesion and/or cohesion failure; those transitions were determined from the nanoscratch traces and plastic deformation. However, the profile at the condition of 400 °C is harder than that of RT due to the ploughed effect from the nanoscratch traces.

From this perspective, the friction traces were relatively reproducible but exhibited greater variability for each sample than that of the original surface (Fig. 2). The changes in the scratch groove morphology indicate the improvements in nano-scale wear resistance, as seen in Fig. 3. This figure is an SPM micrograph, recorded at the end of one of the scratch tracks for each sample, where greater contact pressures and greater penetration have led to large areas of the coating being removed from the scratch track (Fig. 4 and 5) as a result of elastic–plastic deformation. When the penetration is increased, the films start to behave differently as a result of the various annealing temperatures (Figs. 6 and 7).

4. Conclusion

We evaluated the film characteristics of ALD-processed bilayer TiO_2/ZnO on Si substrates using XRD, TEM, and SPM techniques. The TiO_2/ZnO films show obvious oscillations under the friction force in addition to abrupt oscillations and pile-up events at a loading penetration of 30 nm and 21.8 μN for RT, 22.4 μN for 300 °C, and 36 μN for 400 °C. At annealing conditions of 36 μN and 400 °C, the sample exhibits a distinctly higher coefficient of friction with larger debris particles in comparison to that of the RT and 300 °C conditions. A good correlation between the mechanical properties and scratch/wear damage was demonstrated. The higher friction force can be attributed to the intrinsic brittle properties of the ZnO film. Severe plastic ploughing damage, observed at the beginning of wear sliding under a loading penetration of 150 nm, clearly indicates the tip is ploughed across the TiO_2 layer and then reaches the ZnO material. The nanoindentation technique, combined with scratching and friction, has been applied to ALD-processed TiO_2/ZnO films and used to successfully evaluate the film characteristics for a compressive study. The films displayed significant suppression of the lateral indented deformation, inducing the degree of pile-up. Additionally, the setting down, oscillations, and unwanted material can be explained in terms of the stiffness of the film, which depends on the interatomic distances during the scratch tests.

Acknowledgments

This study was supported by the National Science Council of Taiwan (Grant Nos. NSC 101-2221-E-167 -004, NSC 102-2221-E-167 -007, and MOST 103-2221-E-167 -003) and financial support by National Chin-Yi University of Technology (NCUT11-REM-004: 2012.1.1∼2012.10.31 and NCUT 12-REM-003: 2013.1.1∼2013.10.31). We thank Dr. H.C. Wen and Prof. W.C. Chou for the supporting of CL/SEM/EDS/TEM equipment and technical suggestion; Prof. Y.R. Jeng for the supporting the SPM equipment used in this study. We also thank Dr. Ping-Feng Yang and Dr. Yi-Shao Lai for help with the nanoscratch analysis of the samples tests.

References

[1] Philip A, Thomas S, Rajeev Kumar K. Explanation for the appearance of alumina nanoparticles in a cold wall atomic layer deposition system and their characterization. Vacuum 2010;85:368–72.
[2] Knez M, Niesch K, Niinisto L. Synthesis and surface engineering of complex nanostructures by atomic layer deposition. Adv Mater 2007;19:3425–38.
[3] Zhang W, Qiu T, Qu XP, Chu Paul K. Atomic layer deposition of platinum thin films on anodic aluminium oxide templates as surface-enhanced Raman scattering substrates. Vacuum 2013;89:257–60.
[4] Ritala M, Leskela M, Nykanen E, Soininen P, Niinisto L. Growth of titanium dioxide thin films by atomic layer epitaxy. Thin Solid Films 1993;225:288–95.
[5] Yamada A, Sang BS, Konagai M. Atomic layer deposition of ZnO transparent conducting oxides. Appl Surf Sci 1997;112:216–22.
[6] Wen HC, Hung CI, Tsai HJ, Lu CK, Lai YC, Hsu WK. ZnO-coated carbon nanotubes: an enhanced and red-shifted emission band at UV–VIS wavelength. J Mater Chem 2012;22:13747–50.
[7] Hu CJ, Lin YH, Tang CW, Tsai MY, Hsu WK, Kuo HF. ZnO-coated carbon nanotubes: flexible piezoelectric generators. Adv Mater 2011;23:2941–5.

[8] Lu SY, Tang CW, Lin YH, Kuo HF, Lai YC, Tsai MY, et al. TiO_2-coated carbon nanotubes: a redshift enhanced photocatalysis at visible light. Appl Phys Lett 2010;96:231915–7.
[9] Park KS, Seo EK, Do YR, Kim K, Sung MM. Light stamping lithography: microcontact printing without inks. J Am Chem Soc 2006;128:858–65.
[10] Sinha A, Hess DW, Henderson CL. Area-selective ALD of titanium dioxide using lithographically defined poly(methyl methacrylate) films. J Electrochem Soc 2006;153:G465–9.
[11] Gaillot DP, Deparis O, Welch V, Wagner BK, Vigneron JP, Summers CJ. Composite organic–inorganic butterfly scales: production of photonic structures with atomic layer deposition. Phys Rev E 2008;78:031922–6.
[12] Kaidashew EM, von Wenckstern H, Rahm A, Semmelhack HC, Han KH, Benndorf G, et al. High electron mobility of epitaxial ZnO thin films on *c*-plane sapphire grown by multistep pulsed-laser deposition. Appl Phys Lett 2003;82:3901–3.
[13] Dittrich EL, Weidmann J. Electron drift mobility in porous TiO_2 (anatase). Phys Status Solidi A 1998;165:R5–6.
[14] Zhang QF, Dandeneau CS, Zhou XY, Cao GZ. ZnO nanostructures for dye-sensitized solar cells. Adv Mater 2009;21:4087–108.
[15] George SM. Atomic layer deposition: an overview. Chem Rev 2010;110:111–31.
[16] Mohseni H, Scharf TW. Atomic layer deposition of $ZnO/Al_2O_3/ZrO_2$ nanolaminates for improved thermal and wear resistance in carbon–carbon composites. J Vac Sci Technol 2012;30:149–60.
[17] Mohseni H, Mensah BA, Gupta N, Srinivasan SG, Scharf TW. On tailoring the nanocrystalline structure of ZnO to achieve low friction. Tribol Lubric Tech 2012;68:17–9.
[18] Azevedo CR, Marques ER. Three-dimensional analysis of fracture, corrosion and wear surfaces. Eng Fail Anal 2010;17:286–300.
[19] Gagg CR, Lewis PR. Wear as a product failure mechanism – overview and case studies. Eng Fail Anal 2007;14:1618–40.
[20] Sergejev F, Peetsalu P, Sivitski A, Saarna M, Adoberg E. Surface fatigue and wear of PVD coated punches during fine blanking operation. Eng Fail Anal 2011;18:1689–97.
[21] Lin MH, Wen HC, Jeng YR, Chou CP. Nanoscratch characterization of GaN epilayers on *c*- and *a*-axis sapphire substrates. Nanoscale Res Lett 2010;5:1812–6.
[22] Yau WH, Tseng PC, Wen HC, Tsai CH, Chou WC. Luminescence properties of mechanically nanoindented ZnSe. Microelectron Reliab 2011;51:931–5.
[23] Chang YM, Wen HC, Yang CS, Lian D, Tsai CH, Wang JS, et al. Evaluating the abrasive wear of $Zn_{1-x}Mn_xO$ heteroepitaxial layers using a nanoscratch technique. Microelectron Reliab 2011;50:1111–5.
[24] Wu JL, Wu JY, Lee KC, Hsu WK, Lin SJ. Annealed binary nanowires: an efficient creation of abundant oxygen deficient States. J Mater Chem 2011;21:11730–3.
[25] Lee JP, Park MH, Chung TM, Kim Y, Sung MM. Atomic layer deposition of TiO_2 thin films from Ti(OiPr)2 and H_2O. Korean Chem Soc 2004;25:475–9.
[26] Xu LH, Shen H, Li XY, Zhu RH. Enhanced ultraviolet emission from ZnO thin film covered by TiO2 nanoparticles. Chin Opt Lett 2009;7:953–5.
[27] Kim CR, Shin CM, Lee JY, Heo JH, Lee TM, Park JH, et al. Influence of annealing duration on optical property and surface morphology of ZnO thin film grown by atomic layer deposition. Curr Appl Phys 2010;10:S294–7.
[28] Allen MW, Swartz CH, Myers TH, Veal TD, McConville CF, Durbin SM. Bulk transport measurements in ZnO: the effect of surface electron layers. Phys Rev B 2010;81. 075211-075211-6.
[29] Lee JY, Kim CR, Heo JH, Shin CM, Park JH, Lee TM, et al. Effects of buffer layer annealing on ZnO thin films grown by using atomic layer deposition. J Korean Phys Soc 2009;55:2556–9.
[30] Wen HC, Yang CS, Chou WC. Effect of microstructure on the nanomechanical properties of $Zn_{1-x}Cd_xSe$ alloys. Appl Surf Sci 2010;256:2128–31.
[31] Lin TY, Wen HC, Chang ZC, Hsu WK, Chou CP, Tsai CH, et al. Nanoscratch studies of SiGe epitaxial layer damage on the Si substrate. J Phys Chem Solids 2011;72:789–93.
[32] Wu MJ, Wen HC, Wu SC, Yang PF, Lai YS, Hsu WK, et al. Evaluating nanotribological behavior of annealing $Si_{0.8}Ge_{0.2}/Si$ films. Microelectron Reliab 2011;51:2223–7.
[33] Mohseni H, Scharf TW. Atomic layer deposition of $ZnO/Al_2O_3/ZrO_2$ nanolaminates for improved thermal and wear resistance in carbon–carbon composites. J Vac Sci Technol A 2012;30. 01A149-1–01A149-12.